
Disease spread through animal movements: a static and temporal network analysis of pig trade in Germany

Hartmut H. K. Lentz^{1,*}, Andreas Koher², Philipp Hövel^{2, 3}, Jörn Gethmann¹, Carola Sauter-Louis¹, Thomas Selhorst⁴, Franz J. Conraths¹,

1 Institute of Epidemiology, Friedrich-Loeffler-Institute, Südufer 10, 17493 Greifswald, Germany

2 Institute of Physics, Berlin Institute of Technology, Hardenbergstraße 36, 10623 Berlin, Germany

3 Bernstein Center for Computational Neuroscience Berlin, Humboldt-Universität zu Berlin, Philippstraße 13, 10115 Berlin, Germany

4 Unit Epidemiology, Statistics and Mathematical Modelling, Federal Research Institute for Risk Assessment, Alt-Marienfelde 17-21, 12277 Berlin, Germany

* Corresponding Author: hartmut.lentz@fli.bund.de

Abstract

We analyze the network of pig trade in Germany with respect to its ability to spread infectious diseases. We will avoid the usage of external parameters, and restrict ourselves to the measurement of pure properties of the system. These properties do not depend on particular pathogens. These characteristics are on the contrary of great importance for any general spreading process on this particular network. Since the data set under consideration has not been analyzed systematically with respect to a broad spectrum of network measures, the presented work provides a systematic insight into German pig trade network. At the same time, the set of methods used here can be understood as a general framework for a topological-temporal characterization of livestock trade networks.

Introduction

Infections in livestock can spread via various paths. Major transmission routes are (1) geographical closeness to an index premise (aerial transmission) [1–3], (2) vectors (insect, human, appliances) [4] or (3) livestock trade [5–9]. Focussing on the latter, if infectious animals are taken from one premise to another, a disease can be transmitted to the receiving premise. It is therefore crucial to have an understanding of the trade network as a substrate for spreading processes. This analysis focusses on the German pig trade network as a substrate for spreading of infections in pigs. It has been shown that most secondary outbreaks of classical swine fever in Germany in the 1990s were caused by the transport of infected pigs [10].

Contact patterns among hosts forming a contact network are considered as one of the most critical factors contributing to unequal pathogen transmission. During the last decades veterinary epidemiologists have been focussing on the disease transmission between livestock farms. Farms and animal movements between farms can be translated

into nodes and edges of a contact network, respectively. Techniques adopted from social network analysis (SNA) have been intensively applied by veterinary epidemiologists in order to get a better understanding of the spatio-temporal livestock disease dynamics [5, 11–17] and to identify network nodes and edges that are central to the spread of infectious diseases [18, 19].

If nodes and edges differ from one another with respect to their centrality, i.e. with respect to their potential to spread disease, this variability can be used to rank the nodes and edges. Such a ranking allows veterinary authorities to select nodes and edges for the implementation of targeted surveillance and control measures following the central things first rule.

Since data of the analyzed network is not available for public, this article is an attempt to provide a comprehensive picture and characterization of the network itself. Therefore, neither explicit disease specific parameters nor intervention measures are considered. In addition, the analysis provided here can be regarded as a *general framework* to investigate livestock trade networks.

In this work we characterize the static and temporal network of pig trade in Germany as a substrate for spreading processes for the first time. The German pork industry is one of the largest in the world. About 5 million tons of pork meat are produced in Germany every year [20]. The gain in production value is about 7 billion Euros per year [21].

This paper is structured as follows: First we briefly describe the data under consideration. In Section *Static network analysis* we analyze the pig trade data as a static network, where we characterize the network from a large scale perspective and discuss different strategies for targeted vaccination. Section *Weighted network analysis* gives a brief overview of the impact of trade volume on the static network results. We consider the temporal resolution of the network data set in Sections *Network as time series* and *Temporal network analysis*. The network is considered as a time series in Section *Network as time series*. Finally, we take into account causality for network traversal in Section *Temporal network analysis*.

Data

In this article we analyze an extract of the HI-Tier database [22]. The database comprises livestock movements of pigs in Germany since 2006. The extract under consideration represents the trade between premises of the pork production chain in Germany in the period between 2011-01-01 and 2014-12-31. Considered data are owner, prepossessor, trade date and trade volume. Thereof a network was generated, where trading premises are *nodes* that are connected by directed *edges* (trade links). In addition, trade volume can be included as further information giving a weight to each edge of the network. The system consists of elementary pork production chains. Fig. 1 depicts a schematic illustration of the underlying farming system of the network. The figure shows only the production chain of piglet production, raising, fattening and slaughter. Traders and breeding are not shown.

The resulting network will be analyzed in different representations:

1. *Static network*. Direction of trade is taken into account¹. Trade connections are aggregated over time, i.e. the network is static. A trade link is drawn if there is at least one trade action over the observation period. In addition, we analyze the impact of trade volume.

¹In principle, the network could also be considered undirected. However, this approach is less meaningful in this context due to the directed nature of the involved production chain.

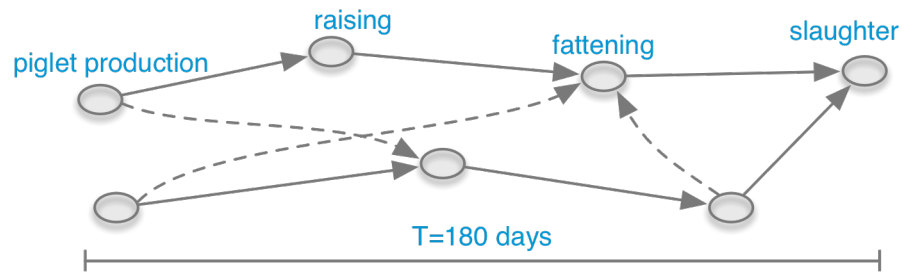


Figure 1. Schematic of pork production chains (solid arrows) in the pig-trade network. Different production chains can be connected by additional cross links (dashed arrows).

2. *Network as time series.* The system is considered as a time series of directed network snapshots at different time steps. Edge weights are considered to some extent.
3. *Temporal network.* The system is considered as a time series of directed network snapshots at different time steps. In addition, causality is fully considered for network traversal via edge sequences.

In each case the network comprises of 97,980 nodes. The static representation (1.) consists of 315,333 edges. For the temporal cases (2.) and (3.) the data set contains 6,359,697 trade transactions (edges). The observation period is $T = 1461 d$, i.e. 1.5 million edges per year.

Analysis

Static network analysis

In this section, we analyze the trade data as a static network. A static network or *graph* $G = (V, E)$ consists of a set of nodes V and a set of edges E , where every edge connects a pair of nodes. In the considered network, edges have a direction given by trade. Mathematically, a network can be represented as an adjacency matrix \mathbf{A} with elements $(\mathbf{A})_{ij} = 1$ if there is an edge from node i to node j , and $(\mathbf{A})_{ij} = 0$ otherwise. The total number of neighbors (trade partners) of a node (premise) is called its *degree* or *total degree*. If edge direction is considered, we distinguish between *in-degree* (incoming edges) and *out-degree* (outgoing edges).

Large scale structure I – Components. In the following, we investigate the component structure of the static network by means of components. We will see that the directed nature of trade plays a major role here.

In principle, the outbreak size of any epidemic on a network is limited by the component structure of the network as a worst case scenario. A *component* is a subset of nodes $C \subseteq V$ for which a path exists between any pair of nodes in C . A *path* $P_{i \rightarrow j}$ between two nodes i and j is an indirect connection between them via arbitrarily many edges without traversing a node twice. Note that for directed networks, $P_{i \rightarrow j}$ does not necessarily imply $P_{j \rightarrow i}$. In general there may exist a large number of paths between two nodes. In this article, by path we always mean the *shortest path*, i.e. the $P_{i \rightarrow j}$ with the smallest number of traversed edges. The average shortest path length in the considered network is 5.5, i.e. on average it takes 5.5 steps to go from a randomly chosen node to another randomly chosen node. The maximum shortest path length is called *diameter* and its value is 18 for the considered network (see Table 1).

Neglecting the directionality of edges, the network exhibits a giant component, which in directed network is commonly called giant weakly connected component (GWCC). For the considered network, it comprises almost all nodes (see Table 1). This means that virtually all nodes of the network are at least 'touched' by trade connections. We find that 99 % of all nodes are connected through trade contacts. Nodes not belonging to the GWCC form other components which are only very small islands in the network.

Table 1. Standard network properties of the static German pig trade network.

Property	Value
Number of nodes	97,980
Number of edges	315,333
Edge density	3.2×10^{-5}
size of GSCC	28 %
size of GWCC	99 %
diameter	18
av. shortest path length	5.5
path density	0.24

The formation of a giant component is also known as percolation and has been studied in a variety of systems [23–25]. From the statistical point of view, a giant component emerges if the number of edges exceeds a certain threshold [25].

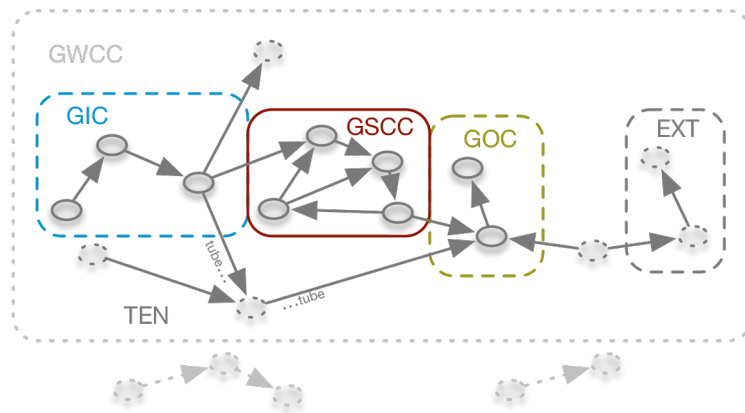


Figure 2. Component structure of directed networks. The giant strongly connected component (GSCC) forms the center of the network (red box). Nodes of the GSCC and the giant in-component (GIC, dashed blue box) have a high spreading potential, whereas all other nodes (GOC - giant out component, dashed yellow box; TEN - tendrils; EXT - external nodes, grey dashed box) cannot reach a significant fraction of the network. Box sizes do not reflect the actual sizes of the components. The giant weakly connected component (GWCC) is given by the grey dotted box.

If edge *direction* is taken into account, the network shows a more complex component structure. This is due to the reciprocity that is not guaranteed in directed networks. The general structure of directed networks has been investigated in [24]. It is schematically depicted in Fig. 2. In analogy to the GWCC, the *giant strongly connected component* (GSCC) is a subset of nodes for which a *directed* path exists between all pairs of them. For the considered data set, the GSCC contains about 1/4 of all nodes

(red box in Fig. 2) and forms the backbone of the network in the sense that it ensures the global connectivity of the network. All nodes with access to the GSCC that are not themselves part of it, form the *giant in-component* (GIC, blue frame in Fig. 2). In analogy, the *giant out-component* (GOC) contains the nodes that can be reached from the GSCC, but are not part of the GSCC themselves (yellow box in Fig. 2).

Besides the mentioned components, a directed network generally contains so-called *tendrils* (TEN, grey dashed nodes in 2). Tendrils are sets of nodes that do not belong to the GSCC, but are reachable from the GIC or that can reach the GOC. A special case of tendrils are *tubes*, which start at the GIC and bypass the GSCC to end in the GOC. Finally, *external node sets* (EXT in Fig. 2) are part of the GWCC, but have no access to the GOC.

Figure 3 shows the distribution of nodes and edges of the different giant structures. About half of the nodes are either in the GSCC or in the GIC. They form the part of the nodes that can in principle cause larger outbreaks. It is remarkable that the GOC makes up only a small part of the network.

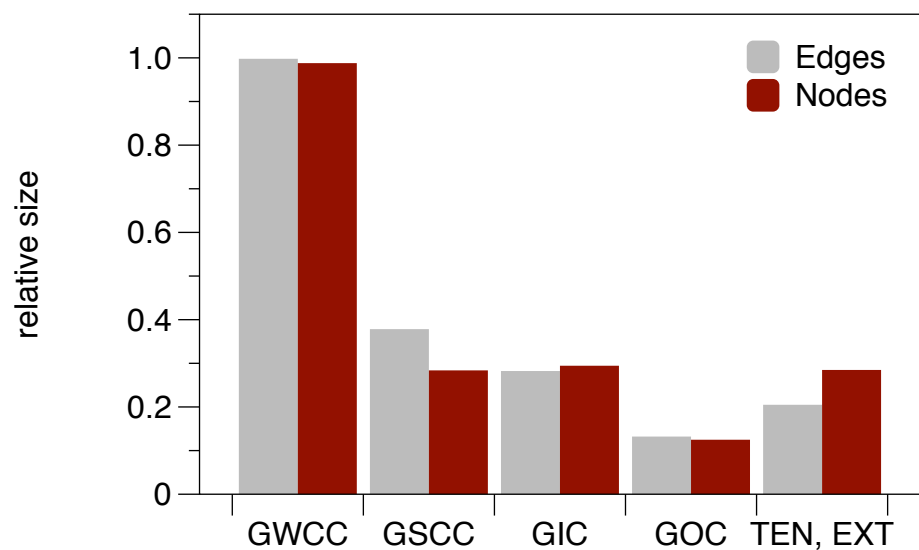


Figure 3. Sizes of the large scale component structure of the pig trade network. Size is normalized to the total number of nodes in the network.

The topology shown in Fig. 2 results in a salient property regarding the spreading potential of the nodes in the network. The spreading potential of a node i can be quantified using the number of nodes reachable from node i by a path of arbitrary length. We call this number the *range* of node i . Therefore, the range of a node defines a simple measure for assessing the risk of a pathogen to spread via the network.

Figure 4 depicts the range of every node in the pig trade network. The distribution shows a strong bimodal structure with two node classes: (i) a class with long-range nodes and (ii) a class with short-range nodes. This distribution can be explained with the component structure as described above: The nodes belonging to the GSCC or GIC have a long range. They make up a fraction of 58 % (56,656 nodes).

All other nodes (GOC, TEN, EXT) show a considerably shorter range. They represent a much smaller risk for the spread of infectious diseases. On the other hand, the maximum range of all short range nodes is still 70.

In principle, tendrils might form large structures as well. The size of these structures can be estimated by removing the GSCC from the network and computing the ranges of the remaining nodes. The maximum range of the tendril nodes is 48 for the pig-trade

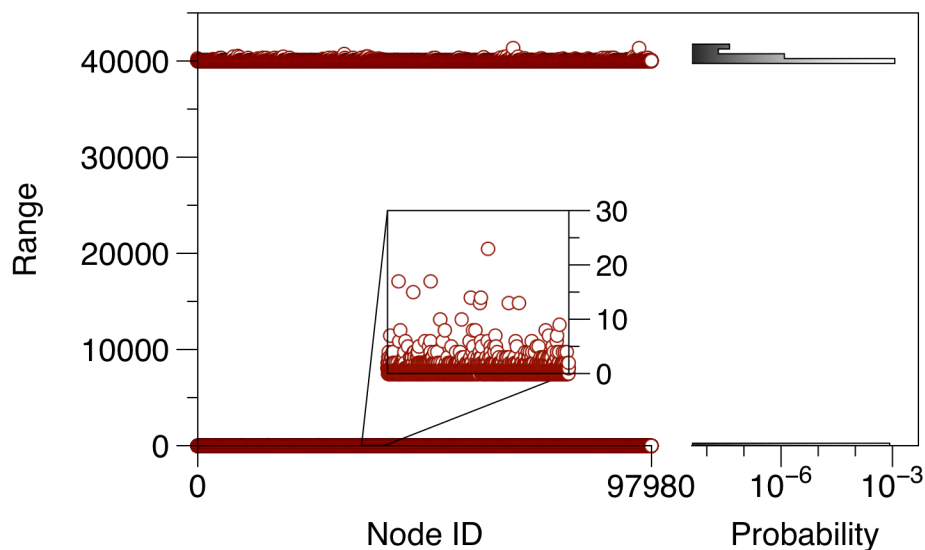


Figure 4. Range for every node in the pig trade network. About 50 % of the nodes have a long range of approximately 40,000 nodes, i.e. an infection started here could reach almost half the network. The other 50 % of the network nodes have a short range and can not cause large outbreaks (maximum short range: 70). The probability distribution of the ranges is shown in the right panel.

network. Nodes of the GOC have a maximum range of 40, whereas EXT nodes can reach up to 70 nodes. Overall, this shows that no large outbreaks can appear in GOC, TEN and EXT. Table 2 shows the maximum ranges in the different giant structures.

Table 2. Maximum ranges for the large scale structures of the network.

Component	Category	Max. range
GIC	long range	41,369
GSCC	long range	40,040
GOC	short range	40
TEN	short range	48
EXT	short range	70

It should be noted that the observed range behavior (Fig. 4) is typical for directed networks. Since (livestock) trade networks are generally directed, a similar behavior can be expected also for other trade networks. Contrary to trade networks, *social* networks, which can be used to model local spreading dynamics, are rather undirected and do not reveal the features shown in Figures 2 and 4.

Large scale structure II – Mixing patterns. In the absence of information on the internal contact structure within a population, a widely used assumption is homogenous mixing. This means that every node could be in contact with any other node in the network and there is no selection bias or characteristic interaction pattern. In this section, we will quantify the strength of mixing structures as they are contained in the pig trade data set. These structures can be arbitrary node categories that have to be defined in the first place (e.g. node type, administrative regions, premise size,

hygiene status, etc.). In the following we restrict our analysis to categories that are intrinsically linked to the data at hand. These are:

1. Federal state
2. District
3. Municipality
4. Degree (number of trade links).

First, we assign a category k to every node in the network, e.g. the federal state in which the node (premise) is located. Then, we compute the number of edges between nodes of the categories (e.g. federal states) k and l . This can be summarized in a mixing matrix \mathbf{e} with elements [26]

$$e_{kl} = \begin{array}{l} \text{number of links between} \\ \text{categories } k \text{ and } l, \end{array} \quad (1)$$

where the indices k and l represent different node categories.

The propensity of a network to prefer links between nodes of the same category can be quantified using the *assortativity coefficient* φ . It is defined as follows [26]:

$$\varphi = \frac{\text{Tr } \mathbf{e} - \|\mathbf{e}^2\|}{1 - \|\mathbf{e}^2\|}, \quad (2)$$

where $\text{Tr } \mathbf{e} = \sum_{i=j} e_{ij}$ is the trace of matrix \mathbf{e} and $\|\cdot\|$ is the sum over all matrix elements. Formally, φ is a correlation coefficient. If a network exhibits a positive assortativity coefficient $\varphi > 0$, it is called an assortative network (with respect to that category); for $\varphi < 0$ the network is called disassortative. Networks where $\varphi = 0$ are called uncorrelated.

Table 3 shows the assortativity coefficients for the four node categories mentioned above. The membership to a federal state represents a large scale classification for each node and the corresponding assortativity coefficient ($\varphi = 0.81$) is relatively high. Premises have thus a preference to trade within the same federal state. As a consequence, imposing trade restrictions along the borders of federal states results in a rather small modification of the original network in case of an outbreak [27].

Fig. 5 shows the contact structure between the federal states in Germany. Nodes are districts that are color-coded according to their federal state membership. Intra-district trade links (self loops) are not shown. Edge widths correspond to the number of trade links between two districts. Node sizes correspond to the node degree. For an improved visualization, edges are bundled for each federal state using the algorithm proposed in [28].

We observe again that the majority of trade takes place within the federal states (intra-district trade links not shown in Fig. 5). Inter-state links are mainly formed between North Rhine-Westphalia (NW) and Lower Saxony (NI) as well as Bavaria (BY) and Baden-Wuerttemberg (BW). In fact, the trade between NW and NI alone accounts for 36% of all inter-state trade connections. The federal states NI, NW, BW und BY account for 47 % of all inter-state edges. The distribution of inter-state trade edges follows the Pareto-Principle, i.e. 20.5 % of the districts contain 80.4 % of the trade links.

Contrary to federal states, there is less tendency that premises trade within their district or municipality (see Table 3). This may originate from the fact that not all types of premises needed for pork production are present in all districts or municipalities.

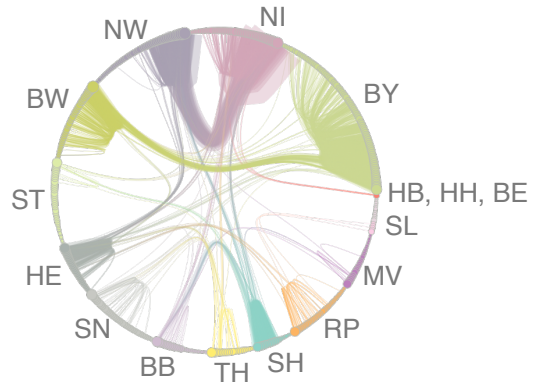


Figure 5. Trade between districts in Germany. Node sizes correspond to the degree. Edges are bundles with respect to the federal states. Trade is dominated by links between districts in NW and NI and BY and BW, respectively. Self-loops (intra-state trade) are not shown.

Table 3. Assortativity coefficients φ of the static German pig trade network. The network is assortative with respect to federal state, district and municipality and disassortative with respect to node degree. σ is a statistical error estimate.

Category	φ	σ
Federal state	0.81	7×10^{-4}
District	0.43	2×10^{-4}
Municipality	0.14	6×10^{-5}
Degree	-0.13	1×10^{-3}

Considering the different mixing categories, the degree plays an important role. It is insightful to investigate whether or not nodes show a tendency to connect with nodes of similar degree. If for example nodes of high in-degree preferably trade with nodes of high out-degree (disassortative network), disease spread would be (at least locally) facilitated. It has been shown that targeted vaccination has a stronger effect in disassortative networks than in uncorrelated or assortative ones [29]. The pig trade network is disassortative with respect to the degree. Table 3 shows the assortativity coefficient for the total degree, which is smaller than zero. Therefore, the pig-trade network is disassortative with respect to this quantity and there is a tendency that nodes of different degree are connected. This behavior is typical for technological and biological networks [29]. Besides the total degree, we also compute φ for all combinations of in-degree and out-degree. The values are similar to the total degree case and are shown in Fig. S3 (Supporting Information).

The standard deviation σ of the mixing coefficient can be estimated statistically [26]. For the considered network all statistical errors are orders of magnitude smaller than the assortativity coefficients (see Table 3). Thus, the observed results are highly statistically significant.

In conclusion, it follows from the analysis of mixing patterns that federal states provide an intrinsic partition of the network, even if this partition is large-scale. In this context, also several federal states could be combined into even larger clusters. Concerning the local mixing structure of the network, we expect that an efficient targeted vaccination is possible, since high-degree nodes tend to be connected to many low-degree nodes. Hence, this analysis can contribute to define regions according to the OIE terrestrial animal health code [30].

Small scale structure - Centrality and intervention allocation. In order to implement efficient measures of disease control and surveillance, the infection risk of every node has to be assessed. For this purpose, so-called centrality measures have been defined. The range defined above is one such centrality measure. We have already shown in Table 2 that the range allows us to identify two risk classes for the nodes in the network.

The simplest centrality measure is the *degree* of a node, which can be easily obtained by counting the number of neighbors. In the case of the pig trade network, we distinguish between in-degree and out-degree; the total number of links a node is connected to is the total degree k . Fig. 6 shows the degree distributions of the network. The figure shows the cumulative distribution on log-scale. The distributions are heavy tailed and the out-degree distribution can be approximated by a power-law, i.e. the distribution has the asymptotic form $p_k \sim k^{-\mu}$ with some constant μ . On the other hand the in-degree distribution exhibits a bimodal structure reflecting the existence of large slaughter houses. It has been shown that the degree distribution has a significant impact on disease dynamics [31–39].

In order to investigate different vaccination strategies for the network, the following centrality measures have been computed:

degree centrality. C_D – Number of neighbors of a node. Normalized to the number of nodes in the network.

betweenness centrality. C_B – Frequency that a node lies on a shortest path between other nodes.

closeness centrality. C_C – Reciprocal average shortest path length between a node and all other nodes.

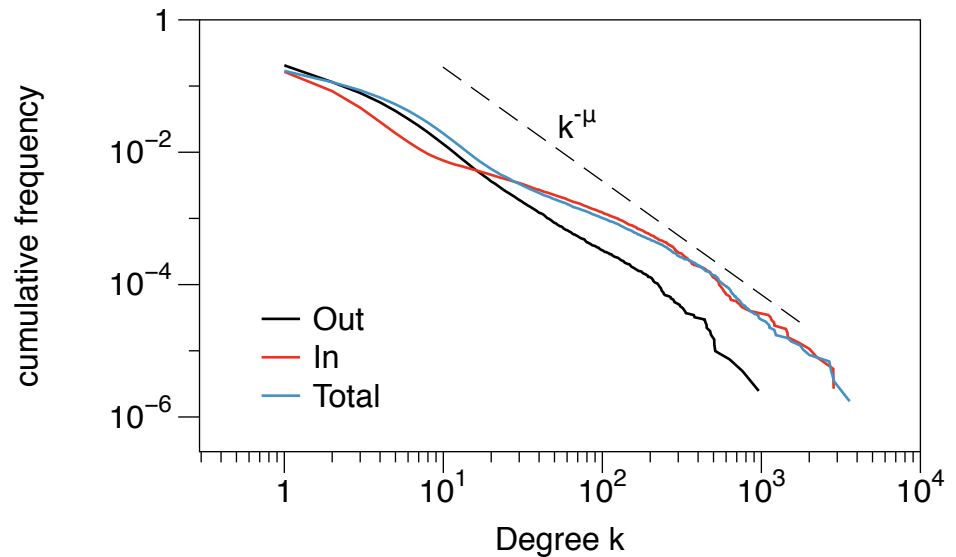


Figure 6. Degree distribution of the livestock trade network. The out-degree distribution can be approximated by a power law of the form $p_k \sim k^{-\mu}$ with $\mu \approx 2.7$ (estimated using a maximum likelihood approach [40]). The figure shows the cumulative distribution to minimize fluctuations.

We also investigate other measures such as eigenvector centrality, pagerank und Katz centrality. These measures, however, turn out to be less suited for disease control (see Section S2, Supporting Information). An overview of the role of different centrality measures for disease control is provided in [12] and [11].

Knowledge of the distribution centrality over the network can be used to implement targeted intervention measures. For this purpose nodes are first of all ranked according to their centrality. Then the impact of the removal of nodes with the highest rank on the functionality of the network can be measured. After each node removal, centrality has to be computed again. In our context, removing nodes does not necessarily mean that they are not active in the trade network, but rather that they effectively can not transmit a disease to other nodes. This can be achieved by culling, isolation of animals, increased hygiene measures or vaccination. The functionality of a network can be defined by the size of its GSCC, since the key feature of every network – namely to ensure the interconnectedness between the nodes – is manifested here. If the size of the GSCC is reduced, the network disintegrates into smaller components and every disease outbreak is restricted to small 'islands'.

The impact of different vaccination strategies on networks has been analyzed in [33,41]. The degree of a node has been shown to be a good indicator for its importance. Furthermore, the degree is relatively easy to measure even if network data knowledge is limited. In addition to the degree we study the suitability of the other centrality measures mentioned above for a risk ranking.

Fig. 7 shows the size of the GSCC depending on the number of removed nodes; nodes are removed according to their centrality rank in decreasing order.

It is remarkable that the removal of randomly chosen nodes barely has a measurable impact on the functionality of the network (dotted line in Figure 7). This phenomenon has also been observed for other systems [33] and is related to the degree distribution of the network. In the case of random removal, about 30,000 nodes must be removed in order to halve the size of the GSCC. For comparison: in case of targeted removal of central nodes it suffices to remove only about 100 nodes to achieve the same effect.

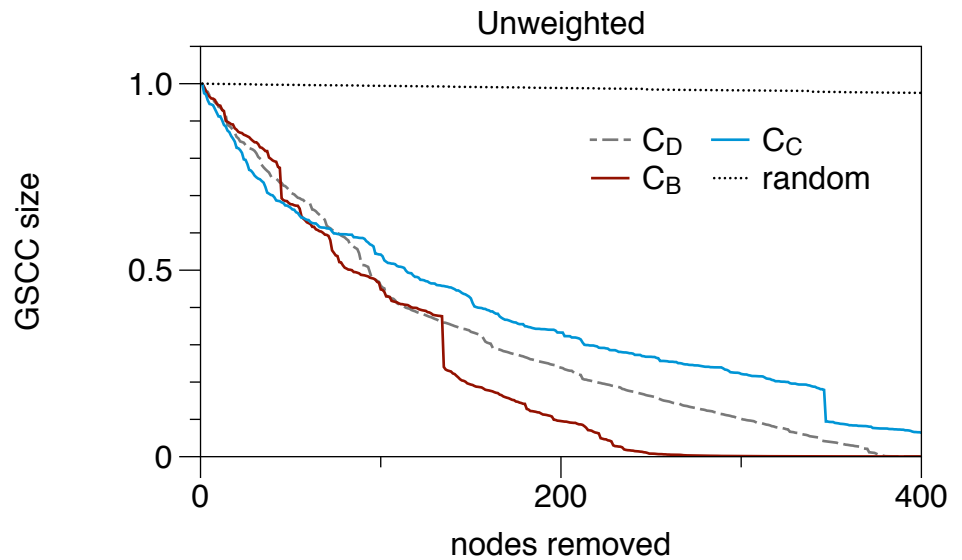


Figure 7. Impact of centrality based node removal, when up to 1 % of the nodes are removed. C_D -Degree centrality, C_B -Betweenness, C_C -Closeness. Size of giant strongly connected component is normalized to unity.

It is apparent from Fig. 7 that the optimal strategy depends on the number of nodes to be removed. In practice this number depends on the specifications of disease control. If about 50 nodes are to be removed from the network, nodes of high closeness or degree should be chosen. In case of removing 100 or more nodes, nodes of high closeness are less efficient. In this case, nodes of high degree and above all nodes with high betweenness should be removed. Overall, betweenness centrality shows the best performance for disease control.

The large-scale structure of the network is also apparent in the distribution of centrality measures. Nodes in the GIC tend to show a high out-degree and low in-degree, whereas the opposite holds for the GOC. One could expect that many high in-degree nodes (slaughter houses) are located in the GOC. Interestingly, nodes with the largest in-degrees are located in the GSCC. These results are provided in Section S3, Supporting Information.

We conclude:

1. any centrality based intervention performs significantly better than random intervention.
2. removal of high closeness or degree nodes is efficient for removal of up to 50 nodes.
3. removal of high betweenness nodes is efficient for removal of more than 100 nodes.

Weighted network analysis

In principle, the number of traded animals plays an important role for the spread of animal diseases, since in reality hardly ever all animals in the outgoing premise are infectious. Depending on the trade volume, this could have a strong impact on the epidemic conductivity, i.e. the infection probability of each edge in the network. Nevertheless, given the relatively high trade volume in the network analyzed here, the mean transmission probability of a trade connection is close to 1 (Section S4, Supporting Information).

On the other hand, there is evidence that the shortest path structure of the network is different for the weighted case. In fact, we find an average shortest path length of 9.7 and a diameter of 30 for the weighted network. Compared to the static network, the average shortest path length is twice as high (see Table 1). This implies that weighted shortest paths differ from purely topologically shortest paths.

Nevertheless, this circumstance does not seem to alter our findings for the unweighted network. We analyze the weighted network with respect to targeted vaccination in Section S4, Supporting Information. The results found are qualitatively similar to the results of the previous section.

In brief, in the context of intervention measures, removing nodes with high trade volume turns out to be an appropriate strategy. Additionally, weighted closeness and weighted betweenness perform well as in the unweighted case. Their performance is, however, not superior to the unweighted case.

Network as time series

In the previous sections, time in the data was aggregated over the whole observation period of four years. This section is devoted to the temporal development of the network. Since the trade system changes over time, we first consider the network as a time series of network snapshots. The temporal resolution of the data set is $\Delta t = 1d$. The time series of the network is given by a sequence of T adjacency matrices

$$\mathcal{A} = \mathbf{A}_1, \mathbf{A}_2, \dots, \mathbf{A}_T, \quad (3)$$

where T is the observation period (here: $T = 1461 d$) and each matrix \mathbf{A}_t is the adjacency matrix of the network at time t (snapshot), i.e. it contains the very edges being active at that time.

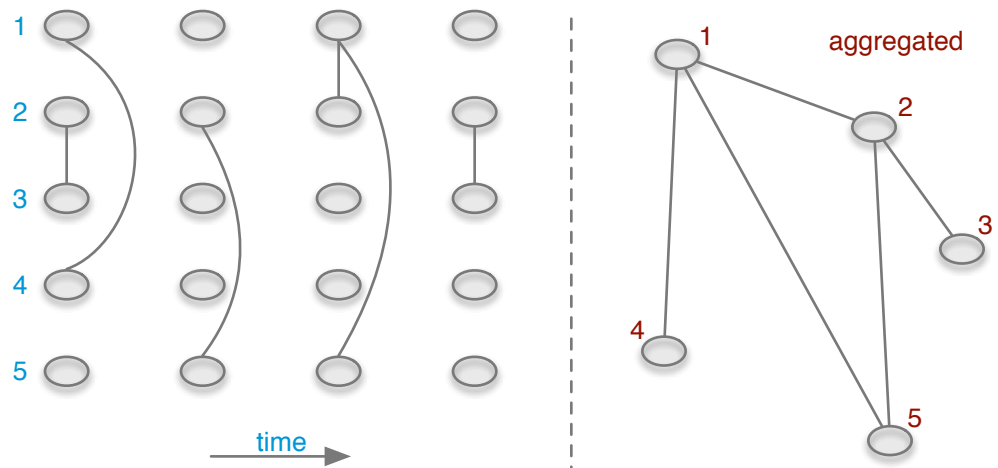


Figure 8. A temporal network (left) and its static counterpart (right).

The static network analyzed above is given by the aggregation over (3). Thus the adjacency matrix of the static network is

$$\mathbf{A} = \sum_{t=0}^T \mathbf{A}_t. \quad (4)$$

This directly applies for the aggregation of trade volumes: for the case of the unweighted network, where volume is not taken into account, the matrices can be

treated as Boolean. This means in effect that every non zero element is set to unity. Fig. 8 shows the aggregation of an exemplary undirected network.

This raises the question how many snapshots \mathbf{A}_t have to be aggregated (size of the aggregation window) in order to recover the properties of the static network as discussed above. The minimum aggregation window has been analyzed for a similar data set (supporting information in [42]). It is roughly one year.

In order to reveal general trends in the temporal evolution of the system, snapshots of the network can be compared at different times. The temporal evolution of the number of edges is shown in Fig. 9 (the figure shows the edge density, i.e. the number of edges normalized by the number of theoretical possible edges). To reduce noise in the data, snapshots have been partially aggregated. The following partial aggregations have been considered: 1 d (yellow), 7 d (weekly, dark blue), 14 d (red), 28 d (monthly, light blue), 84 d (quarterly, grey). For an aggregation window of 84 days we find a linear slope of $10^{-9}d^{-1}$; this corresponds to a decrease of about 3,600 edges per year. The number of active nodes shows a similar trend (Fig. S5, Supporting Information).

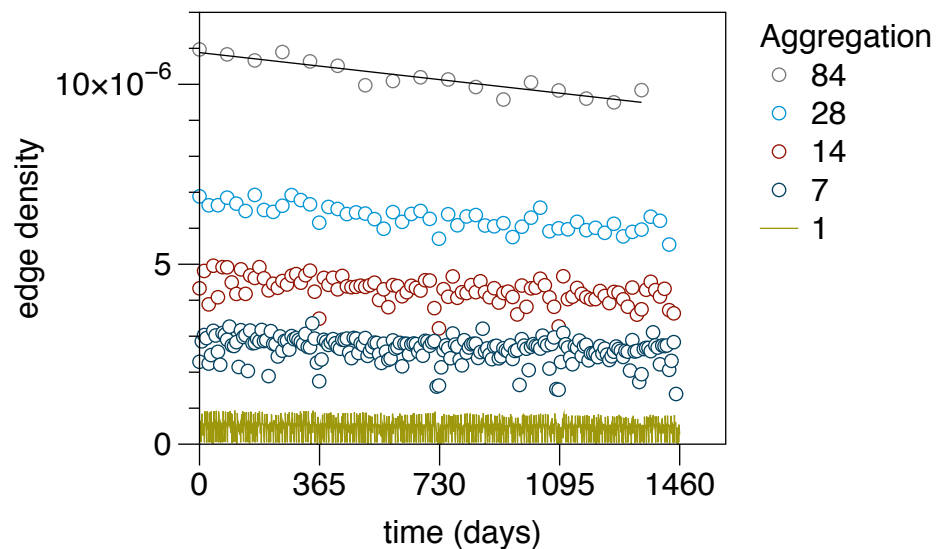


Figure 9. Development of the edge density. There is a clear trend to edge reduction over time. The edge density of the static network is 3×10^{-5} .

Concerning the difference between the static network and the time series, Fig. 9 shows that the edge density of each snapshot is on average less than 10^{-6} . On the other hand, the static network has an edge density of 3×10^{-5} (Table 1). Hence the edge density of the aggregated network is about an order of magnitude higher, i.e. about 10 % of the edges are active every day.

It should be noted that the size of the GSCC is almost unaffected by this trend. This is shown in Fig. 10. The GSCC shows seasonal fluctuations for intermediate aggregation windows (see also [37]). The relatively high stability of the GSCC over time reflects the fact that the network maintains its functionality even though the number of links is reduced over time.

It is important to note that the waiting times in the network are strongly heterogeneously distributed. The waiting times of a node (or edge) are times where the node (or edge) is not active. Fig. 11 shows the distribution of the waiting times of nodes and edges. The figure illustrates that the measured inactivity time spread over several orders of magnitude. Given the shape of the distribution no appropriate mean value can

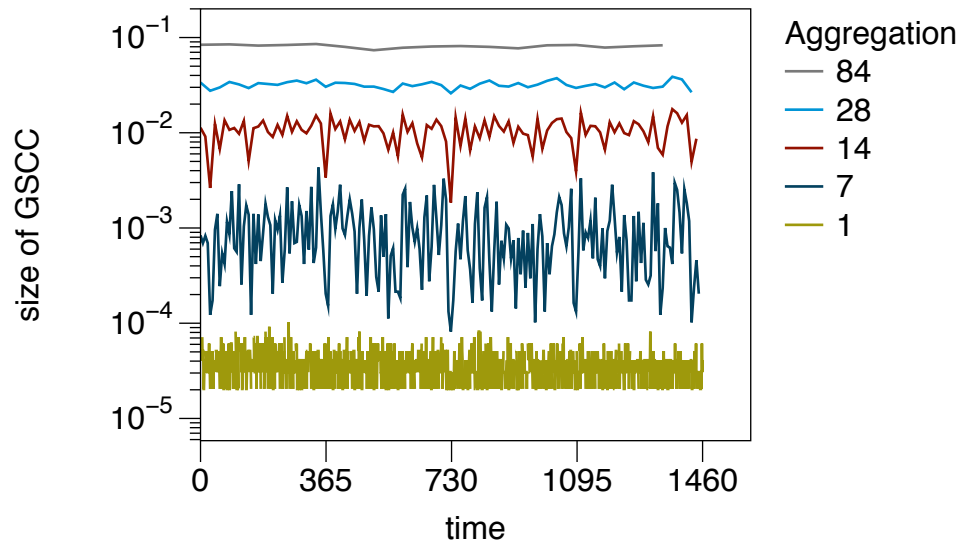


Figure 10. Relative size of the GSCC for different partial aggregation windows. The sizes show stronger seasonal fluctuations on small time scales (red), but remain rather constant over large time scales (grey). Size is normalized by the number of nodes in G .

be given for the waiting times. This is also an indication that an interpretation of the trade links as *rates* between nodes (e.g. the flux of animals between node i and j is m animals per day) is not appropriate for this system. A similar behavior has also been found for other system and is referred to as *bursty behavior* [42–45]. It should be mentioned that for the pig trade network considered here, typical waiting times might be in the system, if premise types were resolved in the data. However, this is not the case for the considered data set and thus the inactivity time reflect a global behavior over all nodes.

In conclusion, nodes and edges can be inactive over a long period of time. This raises the question whether the network can be treated as a static system at all. After all, edges are in fact considered as permanent in the static network. We will address this question in the next section.

Temporal network analysis

In all methods described above the network was either considered as static or partially aggregated snapshots have been treated as static and independent snapshots. However, a closer look reveals that each snapshot is essentially not a meaningful network for disease spread, since typically *indirect* trade connections are not traversed at a single time step. For real network traversal edges at different time steps are necessary.

Thus the network under consideration is in fact a *temporal network*. Existing results and methods from classical social network analysis cannot necessarily be transferred to temporal networks. Overviews of temporal network analysis are provided in [44, 46] and Chapter 4 in [47]. Analyses of epidemic spreading in temporal networks can be found in [42, 45, 48–51].

In this article, we choose a fundamental approach to analyze the pig trade network as a temporal network: The common ground between static networks and temporal networks is the accessibility matrix, i.e. the information whether a node can reach another node via an indirect connection. These connections are called paths.

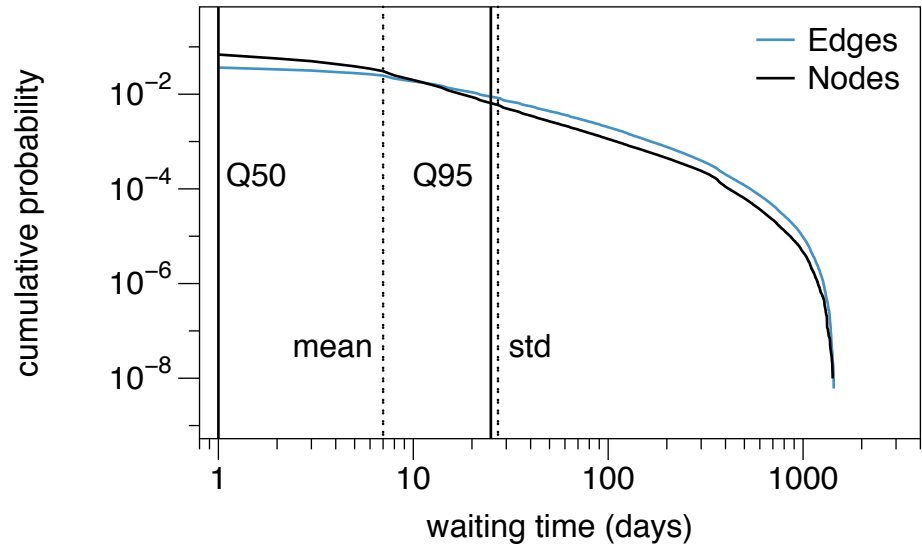


Figure 11. Distribution of node and edge waiting times. The empirical waiting times cover values over three orders of magnitude. Dashed lines show mean and standard deviation of the node waiting times, respectively. Solid lines show median and 95 % quantile of the node waiting time distribution.

Let us first consider a static network $G = (V, E)$. A path $P_{i \rightarrow j}$ from node i to node j is formally given by a sequence of edges between these nodes where the edges can traverse arbitrary other nodes $x_k \in V$, i.e.

$$P_{i \rightarrow j} = [(i, x_1), (x_1, x_2), \dots, (x_n, j)]. \quad (5)$$

The number of steps is the path length. In general, a large number of paths exists between each node pair in a network. For the spread of infectious diseases from node i to node j , only the *shortest path* is of importance, since any longer path between i and j would just correspond to a repeated infection.

In order to take the dynamic nature of trade (in particular heterogeneously distributed waiting times, Fig. 11) into account, every edge of the network has to be tagged with a timestamp. A temporal network is formally given by $\mathcal{G} = (V, \mathcal{E})$, where V is a set of nodes and \mathcal{E} is a set of temporal edges. An edge $(i, j, t) \in \mathcal{E}$ connects nodes i and j at time t . Concerning the static paths defined in Equation (5), an important difference in temporal networks is the fact that successive edges require timestamps that are successive as well. In other words a path in a temporal network has to be *causal*. We refer to a *causal path* from node i to j as $P_{i \rightsquigarrow j}$. Thus, it follows by analogy to (5)

$$P_{i \rightsquigarrow j} = [(i, x_1, t_1), (x_1, x_2, t_2), \dots, (x_n, j, t_n)] \quad (6)$$

with the causality constraint

$$t_1 < t_2 < \dots < t_n. \quad (7)$$

The *path duration* is defined as t_n . Consequently, the shortest path duration from node i to j is that connection where t_n in $P_{i \rightsquigarrow j}$ is minimal.

It is important to emphasize that due to the causality constraint, network traversal cannot be carried over from the static to the temporal case in a straightforward manner. On the other hand, the concept of *accessibility* holds also for the temporal case.

Therefore, we will use this common ground in order to analyze the pig trade in terms of a temporal network.

The accessibility of a static network can be written as a matrix \mathbf{P} with entries:

$$(\mathbf{P})_{ij} = \begin{cases} 1 & \text{es existiert } P_{i \rightarrow j} \\ 0 & \text{else.} \end{cases} \quad (8)$$

The accessibility matrix can be interpreted as the adjacency matrix of the corresponding accessibility graph. For the temporal case, the accessibility matrix \mathcal{P} has the entries:

$$(\mathcal{P})_{ij} = \begin{cases} 1 & \text{es existiert } P_{i \rightsquigarrow j} \\ 0 & \text{else.} \end{cases} \quad (9)$$

Fig. 12 shows an exemplary causal path between nodes i and j . Although there is no causal path from i to k , this path would exist in the static view on the network. If i was the source node of an epidemic outbreak, the epidemic could never reach node k and a static view on the network would overestimate the outbreak size.

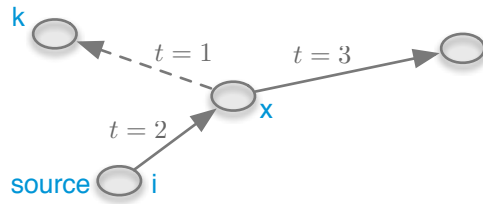


Figure 12. Causal path between nodes i and j in a temporal network. Although the path $P_{i \rightsquigarrow j}$ does not exist in the temporal network, this path exists in the static case.

The authors would like to stress the fact that even in the temporal case the accessibility matrix represents a mathematical graph and is a static quantity. Thus, all concepts above can be transmitted one-to-one from \mathbf{P} (static network) to \mathcal{P} (temporal network).

Computation of the accessibility matrix. Given a *static* network with N nodes the accessibility matrix can be computed as follows [52]:

$$\mathbf{P} \sim \sum_n^N \mathbf{A}^n, \quad (10)$$

where \mathbf{A} is the adjacency matrix of the network. Nevertheless, more efficient methods can be used here [53].

Given a *temporal* network of T time steps, the accessibility matrix (9) can be computed as follows ([54, 55] and Chapter 4.3 in [47]):

$$\mathcal{P} = \prod_{t=1}^T (\mathbf{A}_t + \mathbf{1}), \quad (11)$$

where \mathbf{A}_t is a snapshot of the network at time t (see Equation (3)) and $\mathbf{1}$ is the identity matrix. The accessibility defined in Equation (11) takes the causality of paths into account. Following Equation \mathcal{P} , the entries of the accessibility matrix represent the number of paths between node pairs. In most cases this number is not relevant. Thus, \mathcal{P} can be treated as a Boolean matrix for convenience, i.e. all non zero elements are set to unity.

Range. As we have seen above, the accessibility matrix contains the information, whether an infection started at some node i can reach another node j at all. This has been used implicitly already in Fig. 4, whereby the range of a node i can be computed as $r_i = \sum_j (\mathbf{P})_{ij}$.

This definition can be transferred to the temporal network case in a straightforward manner. Once the accessibility matrix is computed, the (temporal) range of a node is

$$r_i = \sum_j (\mathcal{P})_{ij}. \quad (12)$$

In case of a disease outbreak starting at node i , this quantity gives the number of nodes that can potentially be infected.

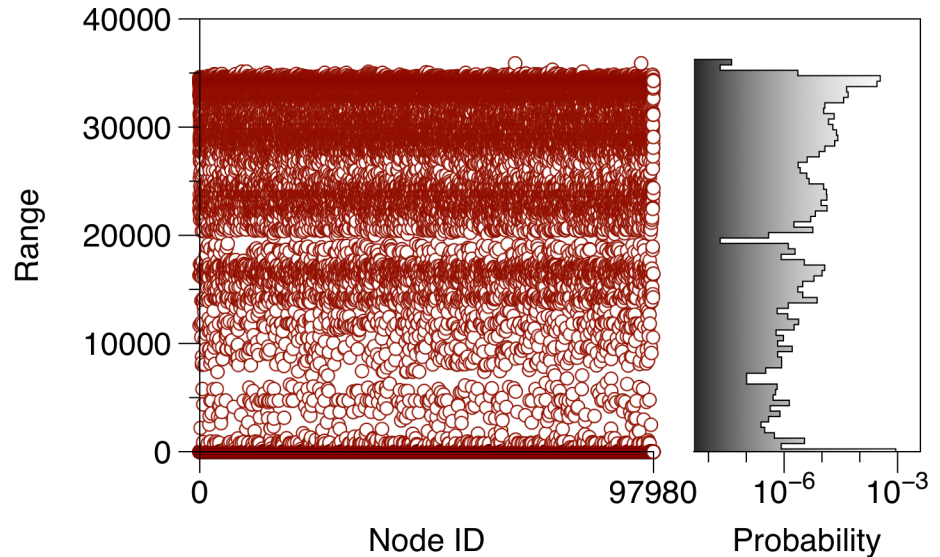


Figure 13. Range for every node in the temporal network. The right panel shows the histogram of the y-axis values on a log scale. In contrast to the static case (see Figure 4) the values cover the whole spectrum from minimum to maximum range.

Fig. 13 shows the range for each node in the temporal pig trade network. The chart is the counterpart to Fig. 4. The bimodal distribution as observed in Fig. 4 is preserved also for the temporal case, although the shape is less pronounced. In contrast to the static case, temporal ranges are observed over the whole spectrum of possible values. This finding suggests that the temporal network does not contain a clear GSCC. In fact, the concept of connectedness in temporal networks is associated with some conceptual problems [46, 56].

The maximum range in the temporal network is 35,905 (for comparison: 41,369 in the static case). On average the temporal range is 17,186.8 (static: 23,154.2). In summary, the average size of an outbreak is overestimated in the static case by almost 35 % and the maximum outbreak size by about 15 %. We will define the error of the static approximation of a temporal network below.

Path density. The number of edges in the accessibility matrix contains important information about a network. In case of the adjacency matrix the number of nonzero elements is up to a constant the edge density of the network². Analogously, the *path*

², i.e. $\rho(\mathbf{A}) = (\sum_{ij} (\mathbf{A})_{ij})/N(N-1)$.

density of a (static) network is given by $\rho(\mathbf{P}) = (\sum_{ij}(\mathbf{P})_{ij})/N^2$. The factor N^2 is chosen since nodes can have a path back to themselves.

For the temporal case, we define the path density:

$$\rho(\mathcal{P}) = \frac{\sum_{ij}(\mathcal{P})_{ij}}{N^2}. \quad (13)$$

The path density takes values between 0 and 1. It should be noted that Equation (13) holds for Boolean matrices³. It contains the information whether a network contains structural holes: In the limit of a high path density, i.e. $\rho(\mathcal{P}) \approx 1$, most nodes can reach each other. On the contrary, for a low path density ($\rho(\mathcal{P}) \approx 0$) the network tends to be temporarily disconnected [56]. For the pig trade network we measure $\rho(\mathbf{P}) \approx 0.24$ for the static case (see table 1) and $\rho(\mathcal{P}) \approx 0.18$ for the temporal case.

Comparison between static and temporal network representation. The static network as described above is just an approximation of the temporal system, where time is aggregated. Aggregation means a removal of causality in paths. As stated above, causality plays an important role for the traversal of temporal networks. This raises the question to what extent a static network approximation maps the real causal accessibility between node pairs correctly.

The difference between the accessibility of a temporal network and its static approximation is illustrated in Fig. 14. If the network is aggregated over time, a path from every node to every other node in the network would be present, i.e. it exists $P_{i \rightarrow j}$ for all nodes i and j including paths from a node back to itself (so-called *self-loops*). For the temporal case the following paths do not exist: $P_{2 \rightarrow 4}$, $P_{3 \rightarrow 4}$, $P_{5 \rightarrow 4}$ and the self-loops $P_{1 \rightarrow 1}$, $P_{4 \rightarrow 4}$ and $P_{5 \rightarrow 5}$. It should be noted that the consideration of self-loops is a matter of definition. In large systems (as the pig trade network) self-loops are statistically irrelevant. In addition, Fig. 14 demonstrates an interesting feature about accessibility graphs of temporal networks: even if the underlying network is undirected, the accessibility graph of a temporal network is generally directed.

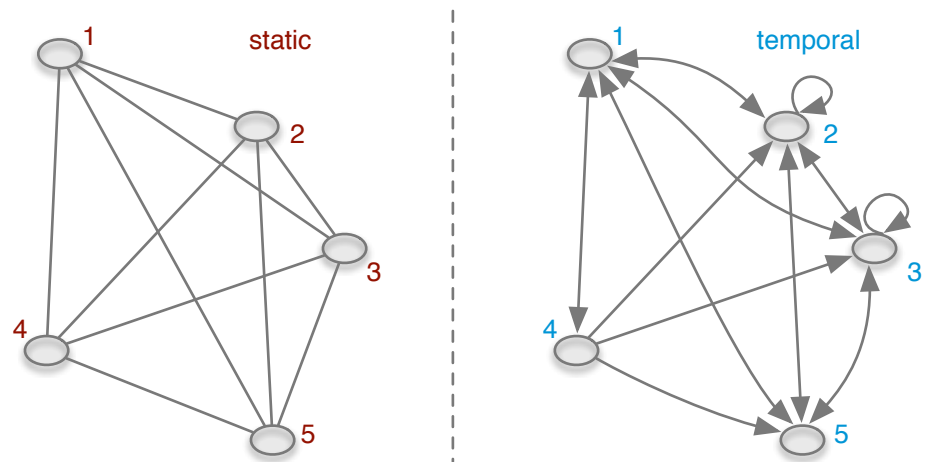


Figure 14. Accessibility graphs of the network of Figure 8. All nodes in the static accessibility graph (left) have a path back to themselves (i.e. self-loops, not shown). Note that although the underlying network is undirected, its accessibility graph is directed.

³In general $\rho(\mathcal{P}) = \text{nnz}(\mathcal{P})/N^2$, where $\text{nnz}(\mathcal{P})$ is the number of non zero elements of \mathcal{P}

In order to quantify the error of the static approximation of a temporal network, the number of paths in the static view can be compared to the number of paths in the temporal system [55]. Their ratio is called *causal fidelity* c , where

$$c = \frac{\sum_{ij} \mathcal{P}_{ij}}{\sum_{ij} \mathbf{P}_{ij}} = \frac{\rho(\mathcal{P})}{\rho(\mathbf{P})} = \frac{\text{number of paths in } \mathcal{G}}{\text{number of paths in } \mathbf{G}}. \quad (14)$$

The number of paths is the number of non zero elements in \mathcal{P} or \mathbf{P} , respectively. A causal fidelity of 1 means that a temporal network is well approximated by a static network. On the other hand, when $c \approx 0$, the network should not be considered as a static system, since most paths are not causal.

In the example in Fig. 14, there are mutual paths between all five nodes (including self-loops), i.e. $\sum_{ij} \mathbf{P}_{ij} = 5^2 = 25$. On the other hand, in the temporal case we have $\sum_{ij} \mathcal{P}_{ij} = 19$ paths. Thus, the causal fidelity is $c = 19/25$.

For the pig trade network, we measure a causal fidelity of

$$c_{\text{pig trade}} = \frac{1,683,966,477}{2,268,652,889} \approx 0.74. \quad (15)$$

This implies that 26 % of the paths that appear to be present in the static network, do not actually exist. As already indicated above, the reciprocal causal fidelity gives an estimation, to what extent a static network view would overestimate a disease outbreak. Therefore, we define the *causal error* of the static network as

$$\epsilon_{\text{pig trade}} = \frac{1}{c_{\text{pig trade}}} \approx 1.35. \quad (16)$$

Consequently, a static approximation of the pig trade network would overestimate the size of a disease outbreak by a factor of 1.35. It should be mentioned that the causal error is not normalized as this is the case for causal fidelity.

Unfolding accessibility. In the previous section, we have discussed how an accessibility graph can be computed. We hereby took into account the whole available time period. Nevertheless there is more information in the accessibility graph. In short, this information can be retrieved if the accessibility matrix is computed step by step and the path density ρ (see (13)) is stored at every step. Hereby, we want to answer the following questions:

1. how can the dynamics of an outbreak be modeled in a temporal network?
2. what is the expected time scale of such an outbreak?

The second question aims at the fact that a temporal network exhibits not only a topological path length, but also a path *duration* (see Equation (7)). It is indeed possible that the average shortest path length of a network is short compared to the network size (see Table 1), but the path duration is very long. In other words, even a short path can take a lot of time. This information is of major interest for disease control since it provides an estimation of the time scale of a disease.

In order to answer the questions above, we consider the accessibility matrix as defined in Equation (11), but we consider T in Equation (11) as the evolving time $t < T$. Hereby, we stepwise store the current result at time t , i.e.

$$\mathcal{P}(t) = \prod_{t'=1}^t (\mathbf{A}_{t'} + \mathbf{1}). \quad (17)$$

Equation (17) yields the temporal evolution of the accessibility. The process of the stepwise computation is referred to as *unfolding accessibility* [55]. Hereby, the focus is on the path *density* since it is a real number (and not a matrix).

Starting at $t = 1$, the matrix $\mathcal{P}(t)$ contains self-loops and the paths to the nearest neighbors. The former is a necessary artifact to allow for paths after inactive periods (see [55] for details). At $t = 2$ the matrix contains all new paths at that time step as well as all former paths and so forth. Thus, the path density grows with every time step. This process mimics an SI-type (susceptible – infected) spreading process with infection probability 1 on the network. That means every causal path is a potential route along which a disease can spread and a node is exposed, whenever it lies on such an infective path.

In analogy to the range defined above (12), the current range $r_i(t)$ of a node i is given by

$$r_i(t) = \sum_j (\mathcal{P}(t))_{ij}. \quad (18)$$

The *herd prevalence* of an SI-process is then given by $r_i(t)/N$. As an example, Fig. 15 shows the current range of a node in the network from Fig. 8.

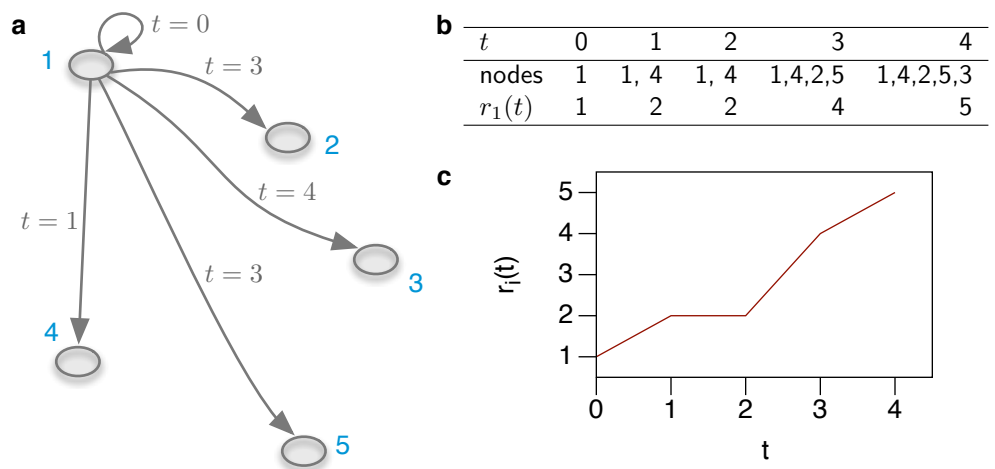


Figure 15. Unfolding accessibility for node 1 in the network shown in Fig. 8. **a** Accessibility of node 1 including time stamps when nodes are accessed. **b** Number of infected nodes over time. **c** Infection curve (i.e. range) for source node 1.

In order to obtain the average herd prevalence $\bar{r}(t)/N$, one can average over all starting nodes, i.e.

$$\bar{r}(t) = \sum_{ij} (\mathcal{P}(t))_{ij} = \rho(\mathcal{P}(t)). \quad (19)$$

Using Equations (18) and (19) the first question is already answered. In short, an SI-process can be modeled by calculating the temporal evolution of the accessibility matrix. Hence, the path density at every time step corresponds to the average herd prevalence over all starting nodes.

In order to answer the second question, we have to find the distribution of path durations. Considering again the new established paths at every time step, $\rho(\mathcal{P}(t = 2))$ for example contains the number of new paths at time $t = 2$ plus the number of paths at $t = 1$ and so forth. In fact, this corresponds to the cumulative distribution of shortest path durations. Consequently, $F_t = \rho(\mathcal{P}(t))/N^2$ is the cumulative distribution function

(CDF) of path durations in a temporal network⁴. The desired shortest path duration distribution is given by dF_t/dt .

Fig. 16 shows the path density (grey solid line) and the probability distribution of shortest path durations (blue dashed line) of the network [55]. The path density corresponds to the mean infection curve. It shows the typical shape of an SI-infection

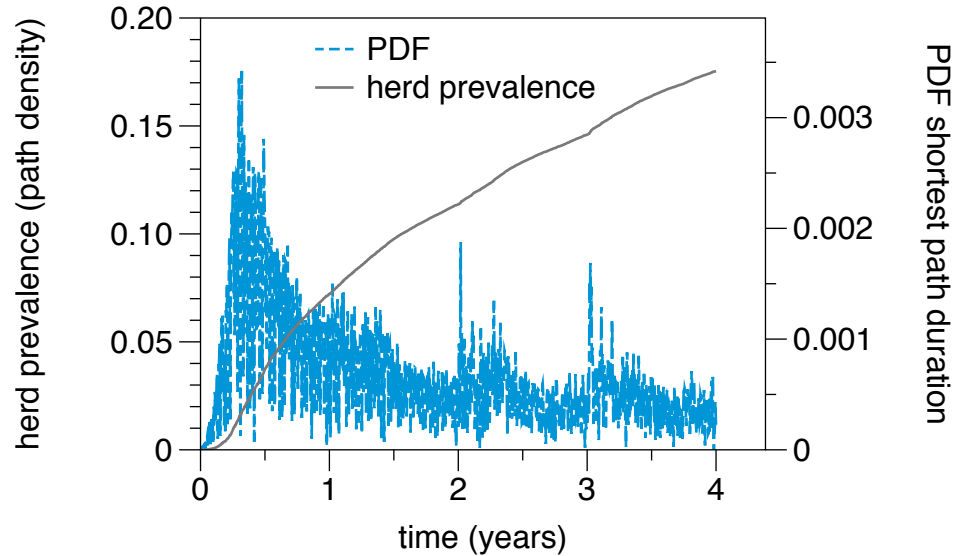


Figure 16. Unfolding accessibility of the temporal pig trade network. The mean herd prevalence (grey solid line) is given by the path density. The probability density function (PDF) of shortest path durations (blue dotted line) shows a global maximum at about 120 days.

curve, although no saturation is reached due to limited observation time in the data set. The shortest path duration (blue dotted line) shows a significant maximum at around half a year. It reaches its peak at about 120 days. This means that an infection spread by pig trade in Germany takes on average 120 days to spread over the network. It is important to stress the fact that this time scale does not depend on any specific disease parameters, but is a pure property of the network as a substrate for spreading. An explanation for this time scale can be found in the structure of the underlying pork production chain (see Figure 1). It defines the temporal diameter of the network (180 days). As observed in Fig. 16, this diameter should limit the distribution of shortest path durations. The maximum is below that value, since there are more possible shorter paths in the production chain than the maximum (longest) path.

Causal contact tracing. The unfolding accessibility method explained above can be used in a straightforward manner for contact tracing in temporal networks. As an addition to existing contact tracing software [57], the method proposed here provides a contact tracing where concepts such as causal error and path density can be analyzed mathematically.

Tracing forward over a certain period τ is equivalent to an accessibility unfolding from the assumed date of entry to $t = \tau$. Using our method, possible paths for infection are computed for all source nodes at once. However, if one is only interested in contact

⁴In this definition the cumulative distribution function is not necessarily normalized. We consider them as 'improper' distribution functions.

premises of one single index premise, the equation for unfolding accessibility (17) can be rewritten accordingly. Let the infection status of the network at time t be given by a row-vector $\mathbf{x}(t)$ with $x_i = 0$, where $x_i = 0$ if node i is susceptible and $x_i \neq 0$ if node i is infected. If node j is the only node infected at the starting time, then the initial vector is $\mathbf{x}(0)$ where $x_j = 1$ and $x_i = 0$ otherwise. The newly infected nodes for every time step are given by the vector

$$\mathbf{i}(t+1) = \mathbf{x}(t+1) - \mathbf{x}(t) = \mathbf{x}(t)\mathbf{A}_t. \quad (20)$$

This equation follows immediately from Equation (17). The sequence $\mathbf{i}(0), \mathbf{i}(1), \dots, \mathbf{i}(t)$ represents the causal tree of possible contacts of the index node up to time t .

In case of a disease outbreak one is also interested in tracing backward. Therefore, the network has to be traversed backwards in time. Here we can again make use of Equation (20), but the network has to be time reversed in the first place. If a temporal network is given by a sequence of adjacency matrices (3), then the time reversed network is

$$\mathcal{A}^{-1} = \mathbf{A}_T^T, \dots, \mathbf{A}_2^T, \mathbf{A}_1^T, \quad (21)$$

where \mathbf{A}_i^T is the transposed of the i -th matrix in the sequence. In other words, the edge direction in each snapshot as well as the temporal ordering of the matrices is reversed. In order to realize a tracing backward, the new adjacency matrix sequence (21) can be used in (20).

Depending on the context, it might be reasonable to allow the traversal to have multiple edges within a single time step. This is the case if there are causal contact chains below the temporal resolution of the network (here $1d$). As an example, a premise could buy animals from farm i in the morning and sell animals to farm j in the afternoon. The path from i to j would not be considered using the approach above. Another example is bad reporting compliance in the sense that multiple transactions might be reported for the same day, but actually happened at multiple points in time. If such circumstances have to be taken into account, we call the tracing procedure *prudent contact tracing*.

In this case, longer static paths have to be considered for every snapshot of the system [54]. Therefore, outbreaks are larger in general. For single nodes, this can have a considerable impact on the number of possible contact nodes. Nevertheless, if the network is considered as a whole, the effect is rather small and results do not change qualitatively (Section S4, Supporting Information).

Summary

In this article, we have analyzed the pig trade network in Germany with respect to its ability to spread infectious diseases. We thereby put a focus on an analysis free of parameters. Thus the obtained results do not depend on specific disease models. Central questions were: (1) what is the big picture of the system and (2) where should efficient disease control measures be located?

On a global scale, the directed nature of trade plays a crucial role: the network exhibits a large scale component structure, which in turn causes a sharp classification of the nodes into two risk classes. Groups of nodes having a large risk of infecting large parts of the system can be found using the ranges of the nodes.

Besides the component structure, the network has a tendency to form subgroups, where little mixing occurs between these subgroups. In particular, the federal states of Germany show such a behavior. In addition, there is a weak tendency for nodes of small degree to connect with nodes of large degree. This fact can be used to make disease control more effective.

The efficiency of disease control measures has additionally been investigated by targeted node removal. For this purpose, different centrality measures have been computed for the nodes in order to obtain a risk based node ranking. We found that it is sufficient to remove 0.1 % of the nodes in order to disassemble the network into small islands. For comparison, in the case of random node removal, 30 % of the nodes would have been required to obtain the same result.

It is necessary for answering the questions above to discuss the depth of the considered data set. In this case, this means the trade volume and the temporal resolution of the data.

As it has turned out, the results hardly change when the trade volume (number of traded animals) is taken into account. We conclude therefore that the relevance of the trade volume is secondary in this context.

The authors would like to emphasize that a static consideration of the network shows significant shortcomings for the understanding of disease dynamics. To begin with, a static network does not contain any time scale by definition. Hence, the duration of an epidemic for example cannot be estimated from the analysis of network topology alone. Considering the network as a series of aggregated snapshots improves the results, but does not take into account causality for infectious trade paths. In addition to that, possible outbreak sizes are systematically overestimated in a static view on the network.

In order to avoid the shortcomings of the static analysis, we continued to regard the system as a temporal network. We thereby took into account the causal occurrences of edges explicitly. Using the unfolding accessibility method, we were able to extract temporal information about a potential epidemic outbreak. This approach mimics an SI-spreading process on the temporal network, where a worst case scenario, i.e. a transmission probability of one is assumed. It is therefore also an appropriate tool for causal contact tracing. Overall, the unfolding accessibility method provides both a large scale view on the network and can be used in order to detect central points in the network.

The expected time for a disease to reach an arbitrary node in the network is 120 days. Even though, it takes on average only 5.5 steps (see Table 1) to traverse the network, these steps take on average 120 days. Thus, the network shows the small world, but also the slow world property.

The error of the static view on the actually temporal system can be quantified using causal fidelity, which compares the possible outbreak sizes in the static and the temporal system, respectively. The causal error of the static network is approximately $\epsilon = 1.35$, i.e. a static view on the network overestimates the outbreak size by 35 %.

Supporting Information

S1 Assortativity coefficients

S2 Targeted vaccination (with Figure S1)

S3 Centrality in components (with Figure S2)

S4 Weighted network (with Figures S3-S4)

S5 Node activity over time (with Figure S5)

S6 Prudent contact tracing (with Figures S6-S7)

Acknowledgements

AK and PH acknowledge funding by the Deutsche Forschungsgemeinschaft in the framework of Collaborative Research Center 910. PH was partially supported by the

Federal Ministry of Education and Research (BMBF), Germany (grant no. 01GQ1001B).

References

1. Mayer D, Reiczigel J, Rubel F. A Lagrangian particle model to predict the airborne spread of foot-and-mouth disease virus. *Atmos Environ*. 2008;.
2. Ducheyne E, De Deken R, Bécu S, Codina B, Nomikou K, Mangana-Vougiaki O, et al. Quantifying the wind dispersal of *Culicoides* species in Greece and Bulgaria. *Geospat Health*. 2007;.
3. Martínez-López B, Ivorra B, Ramos AM, Sánchez-Vizcaíno JM. A novel spatial and stochastic model to evaluate the within- and between-farm transmission of classical swine fever virus. I. General concepts and description of the model. *Vet Microbiol*. 2011;.
4. Olofsson E, Nöremark M, Lewerin SS. Patterns of between-farm contacts via professionals in Sweden. *Acta Veterinaria Scandinavica*. 2014;.
5. Büttner K, Krieter J, Traulsen A, Traulsen I. Static network analysis of a pork supply chain in Northern Germany—Characterisation of the potential spread of infectious diseases via animal movements. *Preventive Veterinary Medicine*. 2013 Jul;110(3–4):418–428. Available from: <http://www.sciencedirect.com/science/article/pii/S0167587713000287>.
6. Fèvre EM, Bronsvoort BMdC, Hamilton KA, Cleaveland S. Animal movements and the spread of infectious diseases. *Trends in Microbiology*. 2006 Mar;14(3):125–131. Available from: <http://www.sciencedirect.com/science/article/pii/S0966842X06000175>.
7. Green DM, Kiss IZ, Kao RR. Modelling the initial spread of foot-and-mouth disease through animal movements. *Proceedings of the Royal Society of London B: Biological Sciences*. 2006 Nov;273(1602):2729–2735. Available from: <http://rspb.royalsocietypublishing.org/content/273/1602/2729>.
8. Ribbens S, Dewulf J, Koenen F, Laevens H, Kruif Ad. Transmission of classical swine fever. A review. *Veterinary Quarterly*. 2004 Dec;26(4):146–155. Available from: <http://dx.doi.org/10.1080/01652176.2004.9695177>.
9. Thrusfield M. *Veterinary epidemiology*. Wiley-Blackwell; 2007.
10. Fritzeimer J. Epidemiology of classical swine fever in Germany in the 1990s. *Vet Microbiol*. 2000;.
11. Martínez-López B, Perez AM, Sánchez-Vizcaíno JM. Social Network Analysis. Review of General Concepts and Use in Preventive Veterinary Medicine. *Transbound Emerg Dis*. 2009;.
12. Dubé C, Ribble C, Kelton D, Mcnab B. A Review of Network Analysis Terminology and its Application to Foot-and-Mouth Disease Modelling and Policy Development. *Transbound Emerg Dis*. 2009;.
13. Bigras-Poulin M, Barfod K, Mortensen S, Greiner M. Relationship of trade patterns of the Danish swine industry animal movements network to potential disease spread. *Prev Vet Med*. 2007;.

-
14. Bigras-Poulin M, Thompson RA, Chriel M, Mortensen S, Greiner M. Network analysis of Danish cattle industry trade patterns as an evaluation of risk potential for disease spread. *Preventive Veterinary Medicine*. 2006 Sep;76(1–2):11–39. Available from: <http://www.sciencedirect.com/science/article/pii/S0167587706000778>.
 15. Christley R, Robinson SE, Lysons R, French NP. Network analysis of cattle movement in Great Britain. In: *Proc. Soc. Vet. Epidemiol. Prev. Med.*; 2005. p. 234–244.
 16. Webb CR. Farm animal networks: unraveling the contact structure of the British sheep population. *Prev Vet Med*. 2005;.
 17. Valdano E, Poletto C, Giovannini A, Palma D, Savini L, Colizza V. Predicting Epidemic Risk from Past Temporal Contact Data. *PLoS Comput Biol*. 2015;.
 18. Natale F, Giovannini A, Savini L, Palma D, Possenti L, Fiore G, et al. Network analysis of Italian cattle trade patterns and evaluation of risks for potential disease spread. *Prev Vet Med*. 2009;.
 19. Natale F, Savini L, Giovannini A, Calistri P, Candeloro L, Fiore G. Evaluation of risk and vulnerability using a Disease Flow Centrality measure in dynamic cattle trade networks. *Prev Vet Med*. 2011;.
 20. Agrarpolitischer Bericht der Bundesregierung 2015. Bundesministerium für Ernährung und Landwirtschaft (BMEL); 2015.
 21. Landwirtschaft verstehen - Fakten und Hintergründe. Bundesministerium für Ernährung und Landwirtschaft (BMEL); 2015. Available from: <http://www.bmel.de/SharedDocs/Downloads/Broschueren/Landwirtschaft-verstehen.html> [cited 2015].
 22. StMELF B. Herkunftssicherungs und Informationssystem für Tiere. ; 2012.
 23. Albert R, Barabási AL. Statistical mechanics of complex networks. *Rev Mod Phys*. 2002;.
 24. Dorogovtsev S, Mendes J, Samukhin A. Giant strongly connected component of directed networks. *Phys Rev E*. 2001;.
 25. Newman MEJ. The Structure and Function of Complex Networks. *SIAM Rev*. 2003;.
 26. Newman MEJ. Mixing patterns in networks. *Phys Rev E*. 2003;.
 27. Lentz HHK, Korschake M, Teske K, Kasper M, Rother B, Carmanns R, et al. Trade communities and their spatial patterns in the German pork production network. *Prev Vet Med*. 2011;.
 28. Holten D. Hierarchical Edge Bundles: Visualization of Adjacency Relations in Hierarchical Data. *Visualization and Computer Graphics, IEEE Transactions on*. 2006 Sept;12(5):741–748.
 29. Newman MEJ. Assortative Mixing in Networks. *Phys Rev Lett*. 2002;.
 30. OIE. Terrestrial Animal Health Code. 24th ed. OIE; 2015.
 31. Pastor-Satorras R, Vespignani A. Epidemic dynamics in finite size scale-free networks. *Phys Rev E*. 2002;.

-
32. Pastor-Satorras R, Vespignani A. Epidemic dynamics and endemic states in complex networks. *Phys Rev E*. 2001;.
 33. Albert R, Jeong H, Barabási AL. Error and attack tolerance of complex networks. *Nature*. 2000;.
 34. Danon L, Ford AP, House TA, Jewell CP, Keeling MJ, Roberts GO, et al. Networks and the Epidemiology of Infectious Disease. *Interdiscip Perspect Infect Dis*. 2011;.
 35. Lloyd AL, May RM. Epidemiology. How viruses spread among computers and people. *Science*. 2001;.
 36. Jones JH, Handcock M. Social networks: Sexual contacts and epidemic thresholds. *Nature*. 2003;.
 37. Kao RR, Danon L, Green DM, Kiss IZ. Demographic structure and pathogen dynamics on the network of livestock movements in Great Britain. *Proc R Soc B*. 2006;.
 38. Schwartz N, Cohen R, ben Avraham D, Barabási AL, Havlin S. Percolation in directed scale-free networks. *Phys Rev E*. 2002;.
 39. Meyers L, Pourbohloul B, Newman MEJ. Network theory and SARS: predicting outbreak diversity. *J Theor Biol*. 2005;.
 40. Clauset A, Newman MEJ. Power-Law Distributions in Empirical Data. *SIAM Rev*. 2009;.
 41. Holme P, Kim BJ, Yoon CN, Han SK. Attack vulnerability of complex networks. *Phys Rev E*. 2002;.
 42. Korschake M, Lentz HHK, Conraths FJ, Hövel P, Selhorst T. On the Robustness of In- and Out-Components in a Temporal Network. *PLOS ONE*. 2013;.
 43. Pan RK, Saramäki J. Path lengths, correlations, and centrality in temporal networks. *Phys Rev E*. 2011;.
 44. Holme P, Saramäki J. Temporal networks. *Phys Rep*. 2012;.
 45. Bajardi P, Barrat A, Natale F, Savini L, Colizza V. Dynamical patterns of cattle trade movements. *PLOS ONE*. 2011;.
 46. Casteigts A, Flocchini P, Quattrociochi W, Santoro N. Time-varying graphs and dynamic networks. *Int J Parallel Emergent Distrib Syst*. 2012;.
 47. Lentz HHK. Paths for epidemics in static and temporal networks. Humboldt-University of Berlin; 2013.
 48. Rocha LEC, Liljeros F, Holme P. Simulated Epidemics in an Empirical Spatiotemporal Network of 50,185 Sexual Contacts. *PLoS Comput Biol*. 2011;.
 49. Valdano E, Ferreri L, Poletto C, Colizza V. Analytical Computation of the Epidemic Threshold on Temporal Networks. *Phys Rev X*. 2015;.
 50. Bajardi P, Barrat A, Savini L, Colizza V. Optimizing surveillance for livestock disease spreading through animal movements. *J R Soc Interface*. 2012;.
 51. Vernon MC, Keeling MJ. Representing the UK's cattle herd as static and dynamic networks. *Proc R Soc B*. 2009;.

-
52. Warshall S. A theorem on boolean matrices. *J ACM*. 1962;.
 53. Skiena SS. *The Algorithm Design Manual*. 2nd ed. Springer Publishing Company, Incorporated; 2008.
 54. Grindrod P, Parsons M, Higham D, Estrada E. Communicability across evolving networks. *Phys Rev E*. 2011;.
 55. Lentz HHK, Selhorst T, Sokolov IM. Unfolding Accessibility Provides a Macroscopic Approach to Temporal Networks. *Phys Rev Lett*. 2013;.
 56. Nicosia V, Tang J, Musolesi M, Russo G, Mascolo C, Latora V. Components in time-varying graphs. *Chaos*. 2012;.
 57. Nöremark M, Widgren S. EpiContactTrace: an R-package for contact tracing during livestock disease outbreaks and for risk-based surveillance. *BMC Veterinary Research*. 2014;.